RSC Advances

PAPER

View Article Online
View Journal | View Issue

Cite this: *RSC Adv.*, 2017, **7**, 4453

Sulfur-alloyed Cr_2O_3: a new p-type transparent conducting oxide host

Samira Dabaghmanesh,*[abc] Rolando Saniz,[a] Erik Neyts[b] and Bart Partoens[a]

Received 6th December 2016
Accepted 27th December 2016

DOI: 10.1039/c6ra27852c

www.rsc.org/advances

Doped Cr_2O_3 has been shown to be a p-type transparent conducting oxide (TCO). Its conductivity, however, is low. As for most p-type TCOs, the main problem is the high effective hole mass due to flat valence bands. We use first-principles methods to investigate whether one can increase the valence band dispersion (*i.e.* reduce the hole mass) by anion alloying with sulfur, while keeping the band gap large enough for transparency. The alloying concentrations considered are given by $Cr_4S_xO_{6-x}$, with $x = 1$–5. To be able to describe the electronic properties of these materials accurately, we first study Cr_2O_3, examining critically the accuracy of different density functionals and methods, including PBE, PBE+U, HSE06, as well as perturbative approaches within the GW approximation. Our results demonstrate that $Cr_4S_2O_4$ has an optical band gap of 3.08 eV and an effective hole mass of 1.8 m_e. This suggests $Cr_4S_2O_4$ as a new p-type TCO host candidate.

1 Introduction

There exist many theoretical and experimental studies on transparent conducting oxides (TCOs). The interest stems mainly from the fact that these materials offer both optical transparency and electrical conductivity for optoelectronics applications. According to the type of carriers that mainly contribute to the conductivity, the TCOs are divided into p-type, *i.e.* hole conducting, and n-type, *i.e.* electron conducting. To date, the n-type TCOs, with application in optoelectronic devices, solar cells, organic light emitting diodes (OLEDs), and sensors, see ref. 1 and references therein, have received more attention rather than p-type's. However, advanced applications of TCOs requiring p–n junctions, such as the active electronic devices, bipolar transistors and diodes, are still severely limited due to the lack of efficient p-type TCOs.[1,2]

Generally, p-type TCOs suffer from low conductivity compared to their n-type counterparts. In contrast to the latter, developing a p-type TCO has always been challenging. The main reason for the low hole conductivity in most of these oxides is that the top of the valence band is dominated by oxygen p-states, which are highly localized and lead to flat bands and consequently a large effective hole mass.[3]

The $CuAlO_2$ delafossite was reported by Kawazoe *et al.*[4] as the first TCO with p-type conductivity and transparency in the visible range. This study opened a route to look for further p-type Cu-delafossites structures such as $CuMO_2$ M ∈ {Ga, Sc, B, Cr}.[5–8] The highest p-type conductivity, 220 S cm^{-1} (resistivity of 0.45×10^{-2} Ω cm), in this family has been reported in the case of Mg-doped $CuCrO_2$ ($CuCrO_2$:Mg).[8] In comparison with the best reported n-type TCO, Sn-doped In_2O_3, with a conductivity of the order of 10^4 S cm^{-1} (ref. 9), this amount of conductivity is very low. The spinel $ZnRh_2O_4$ (ref. 10) and distorted delafossite $SrCu_2O_2$ (ref. 11) are the other examples of p-type TCOs, with conductivities of 2.75 S cm^{-1} and 0.053 S cm^{-1} respectively.

Cr_2O_3 has been considered as a candidate p-type TCO host in several studies. Doping with Ni[12–14] and with Li[13,15] have been shown to induce p-type conductivity in Cr_2O_3. Cr_2O_3:N has received attention for applications in optoelectronic devices, in particular, as hole transporting layer in organic solar cells.[16,17] Farrell *et al.*[18] investigated the possibility of using dopants to create a p–n homojunction with Cr_2O_3. These authors studied the influence of Mg dopants and oxygen pressure in Cr_2O_3 as a p-type TCO.[18] Arca *et al.*[19,20] used a co-doping mechanism to obtain a Cr_2O_3-based p-type TCO. They investigated the conductivity and transparency of Cr_2O_3 by co-doping with Mg and N impurities. They found a resistivity of 3 Ω cm and an optical transmission up to 65% for a 150 nm thick Cr_2O_3 film. These properties are low compared to those reported for $CuCrO_2$:Mg and n-type TCOs.

Chromia, Cr_2O_3, has the corundum structure, with a rather large experimental optical gap of 3.3–3.4 eV.[21,22] However, the flat non-dispersed nature of the valence band of Cr_2O_3 causes a large hole effective mass, of the order of 12–13 m_e at the valence band maximum (VBM),[23,24] resulting in the relatively poor conductivity of doped Cr_2O_3.

A general idea to improve the p-type conductivity in oxides was proposed by Hosono in 2007.[3] He proposed to increase the

[a]Department of Physics, University of Antwerp, Groenenborgerlaan 171, B-2020 Antwerpen, Belgium. E-mail: samira.dabaghmanesh@uantwerpen.be
[b]Department of Chemistry, University of Antwerp, Universiteitsplein 1, B-2610 Antwerp, Belgium
[c]SIM vzw, Technologiepark 935, BE-9052 Zwijnaarde, Belgium

VB dispersion by anion alloying, *i.e.*, forming hybridized orbitals between O 2p states and chalcogen p orbitals (S, Se, and Te) which are more delocalized than O 2p orbitals. The hybridization is expected to lead to an increase in the VB dispersion, resulting in a smaller effective hole mass and, consequently, a higher mobility and conductivity. In this study we follow this idea to try to find new Cr_2O_3-based p-type TCO host candidates. We use first-principles techniques to investigate the effect of partially substituting oxygen atoms with sulfur. Since our main goal is to improve Cr_2O_3 as a p-type TCO host, we should keep in mind that increasing the VBM dispersion may close the gap and reduce the optical transparency of the host. In order to obtain both critical properties for a p-type TCO host, *i.e.* a large enough band gap (larger than 3 eV) and low hole mass, we consider different concentrations of sulfur. Applying state of the art *ab initio* techniques we study the compounds $Cr_4S_xO_{6-x}$, with $x = 1$–5. The most advantageous properties are obtained for $x = 2$, $Cr_4S_2O_4$, having a much lower hole effective mass (1.8 m_e) than Cr_2O_3 (12–13 m_e), and with a gap still larger than 3 eV (3.08 eV).

The paper is organized as follows: in Section 2 we present the methods and approaches we used in our work. In Section 3 we discuss the results and we end the paper with concluding remarks in Section 4.

2 Methods

Within a density functional theory (DFT) approach and using the plane-wave basis sets and the projector augmented-wave method[25] we obtain the structural and electronic properties of Cr_2O_3 and $Cr_4S_xO_{6-x}$ ($x = 1$–5) compounds. All the calculations were performed using the VASP (Vienna Ab-initio Simulation Package) code.[26–29] To the best of our knowledge, there exist no experimental data for any of the $Cr_4S_xO_{6-x}$ cases in the literature to compare with. In order to select the best computational scheme for the $Cr_4S_xO_{6-x}$ cases, we first examine various approaches for Cr_2O_3 and compare the results with experiment. The spin polarized generalized gradient approximation of Perdew–Burke–Ernzerhof (PBE) is used for the exchange correlation functional.[30] In order to correct the strong correlation effects in the partially occupied Cr d states a +U correction is used in the form proposed by Dudarev *et al.*[31] First, we performed geometry optimization, total energy, band structure and density of states calculations based on PBE and PBE+U. We used various U parameter values, as proposed in previous studies on Cr_2O_3,[23,32,33] and compared them with the results obtained with the hybrid functional approach proposed by Heyd, Scuseria, and Ernzerhof (HSE)[34] with the screening parameter $\mu = 0.2$ Å^{-1} (HSE06).[35] Next we compared all PBE, PBE+U, and HSE06 results with two levels of approximation within the perturbative GW approach,[36] as implemented in the VASP code.[37,38] In the first level, Kohn–Sham eigenvalues and eigenfunctions are used to compute the Green's function G and screened Coulomb interaction W in a single step (G_0W_0). In the second level, the eigenvalues in the Green's functions are updated self consistently ($scGW_0$). In the case of PBE, PBE+U, and HSE06 we used a $8 \times 8 \times 8$ k-point grid for total energy and structure optimization calculations, and a $21 \times 21 \times 21$ grid for the density of states calculations. A cutoff energy of 500 eV was used for the plane-wave basis set. Both lattice parameters and atom coordinates are relaxed. For the electronic structure calculation we considered the results as converged when the energy difference between two successive steps was smaller than 10^{-6} eV and for the geometry optimization we considered a convergence criterium for the forces on the atoms of less than 0.01 eV Å^{-1}. For the GW calculations, a $4 \times 4 \times 4$ k-point grid was used. Convergence of the band gap was checked. The number of bands was increased to 1500 in GW calculations based on the convergence test. In the partially self-consistent GW ($scGW_0$), four steps were found to be enough for the convergence of the band gap energy within 0.01 eV.

3 Results and discussion

3.1 Cr_2O_3

Cr_2O_3 has a rhombohedral primitive cell with 2 formula units, *cf.* Fig. 1(a). Oxygen atoms form a hexagonal close-packed structure while Cr atoms occupy two-thirds of the interstitial octahedral sites.[41] In its ground state, Cr_2O_3 adopts the $R3c$ structure[42,43] and is antiferromagnetic (AFM), with a Néel temperature of 308 K.[44] The magnetic structure corresponds to a + − + − spin sequence on the Cr atoms along the c-axis.[41,45]

The calculated lattice constants, magnetic moments, and direct band gap, calculated with the different DFT methods mentioned above, are compared with experiment in Table 1. For the PBE+U calculations we employed U parameters as proposed in the ref. 23, 32 and 33. Ref. 32 proposed $U = 3$ eV and ref. 33 used $U = 5$ eV and $J = 1$ eV for the on-site Coulomb-repulsion and exchange integral for the Cr d electrons. In ref. 23, the authors proposed a +U correction of $U_{Cr_d} = 3$ eV and $U_{O_p} = 5$ eV for the Cr 3d and O 2p states by comparing the electronic density of states (EDOS) of Cr_2O_3 with their experimental spectra obtained using ultra violet photoemission spectroscopy and X-ray photoemission spectroscopy. The PBE and PBE+U methods tend to overestimate the lattice parameters while underestimating the band gap compared to experiment. We compared the band structure and density of states obtained using three U parameter values with experiment. The experimental valence band-width, measured by XPS, is about 9 eV

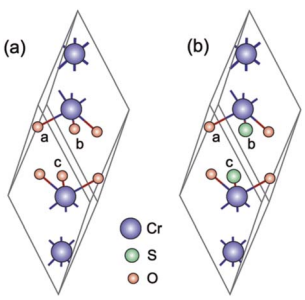

Fig. 1 (a) Unitcell of Cr_2O_3 (rhombohedral) and (b) $Cr_4S_2O_4$ (monoclinic). The purple, red, and green spheres represent chromium, oxygen, and sulfur, respectively.

Table 1 Optimized lattice parameters a and α in Å and degree, magnetic moments, and direct band gap E_g in eV, of the Cr_2O_3 bulk, for different DFT functionals, PBE, PBE+U, HSE06 and experimental values

Method	a	α	μ	E_g
PBE	5.40	54.12	2.51	1.44
PBE+U ($U_{Cr_d} = 3$)	5.42	55.08	2.78	2.60
PBE+U ($U_{Cr_d} = 5$)	5.43	55.19	2.83	2.89
PBE+U ($U_{Cr_d} = 3$, $U_{O_p} = 5$)	5.40	55.01	2.80	2.80
HSE06 ($\alpha = 0.17$)	5.36	55.15	2.85	3.4
Experiment	5.35 (ref. 39)	55.12 (ref. 39)	3.8 (ref. 40)	3.4 (ref. 21 and 22)

with a small (second) gap inside the VB.[23,46–49] We found that $U_{Cr_d} = 3$ eV and $U_{O_p} = 5$ eV, proposed in ref. 23, gives a larger band gap, wider band width (*i.e.* almost 6 eV), and narrower second gap inside the valence band compared to the other U parameters and in better agreement with experiment. Henceforth, we use these U parameters for all our results in the case of PBE+U calculations. Fig. 2 and 3 show the band structures, total EDOS and partial density of states PEDOS of Cr_2O_3 calculated with the PBE, PBE+U, and HSE06 approximations. Since HSE06 overestimates the band gap (by about 1 eV) using the standard Hartree–Fock mixing parameter ($\alpha = 0.25$), we tuned the α parameter. We found that the optimized value $\alpha = 0.17$ gives the experimental band gap (3.4 eV). The calculated VB width obtained by HSE06 (about 7.22 eV) is wider than the PBE and PBE+U methods, in better agreement with experiment. HSE06 also gives the second gap in good agreement with the DOS obtained by Robertson *et al.* using the screened exchange (sX) hybrid density functional.[50] In order to find a reliable predictor for the band gap of the $Cr_4S_xO_{6-x}$ compounds, we also calculate the band gap of Cr_2O_3 using two flavors of the GW approximation, G_0W_0 and $scGW_0$, as indicated above. We used as input for these the eigenvalues and eigenfunctions of both PBE and PBE+U. In Table 2 we summarize our results. Clearly, G_0W_0 largely overestimates the band gap whenever PBE+U results are used as the starting point, independently of the U values used. On the other hand, the band gap is underestimated when PBE results are used as a starting point. Updating G self-consistently ($scGW_0$) on top of PBE as the staring point gives the direct band gap of 3.55 eV, which is close to HSE06 and experimental

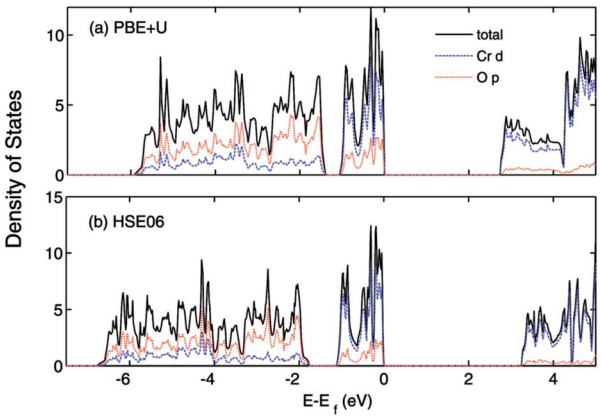

Fig. 3 (a) PBE+U ($U_{Cr_d} = 3$ eV, $U_{O_p} = 5$ eV) and (b) HSE06 calculated total (states per eV per unitcell) and partial (states per eV per atom) density of states of Cr_2O_3. The VBM is aligned to 0.

results. We also performed $scGW_0$ on top of PBE+U, using the optimum U values mentioned before, and found a largely overestimated band gap of 4.489 eV. Fig. 4 shows the $scGW_0$ quasiparticle energies (red dots) for several k-points on top of PBE band structure (blue lines). We see that $scGW_0$ opens the gap by moving both the conduction and valence bands, up and down respectively. $ScGW_0$ on top of PBE gives the wider band width (about 7.45 eV) compared to PBE, PBE+U, and HSE06 approaches, and closer to experiment. Also, the PBE second band gap tends to be closed by $scGW_0$, again bringing it closer to experiment. Comparing these key properties, band gap, band

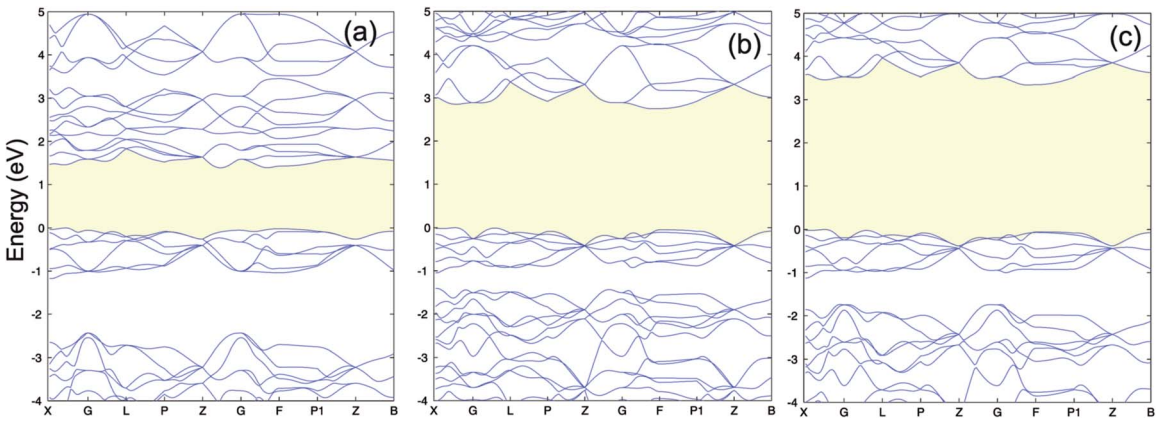

Fig. 2 (a) PBE (b) PBE+U ($U_{Cr_d} = 3$ eV, $U_{O_p} = 5$ eV) and (c) HSE06 band structure of Cr_2O_3. The VBM is set to 0.

Table 2 Direct band gap in eV of the Cr_2O_3 bulk, calculated with single shot G_0W_0 and partially self consistent $scGW_0$ using different approximations as the starting point

Method	G_0W_0	$scGW_0$
PBE	2.845	3.556
PBE+U ($U_{Cr_d} = 3$)	4.20	—
BE+U ($U_{Cr_d} = 5$)	4.58	—
PBE+U ($U_{Cr_d} = 3$, $U_{O_p} = 5$)	4.238	4.489

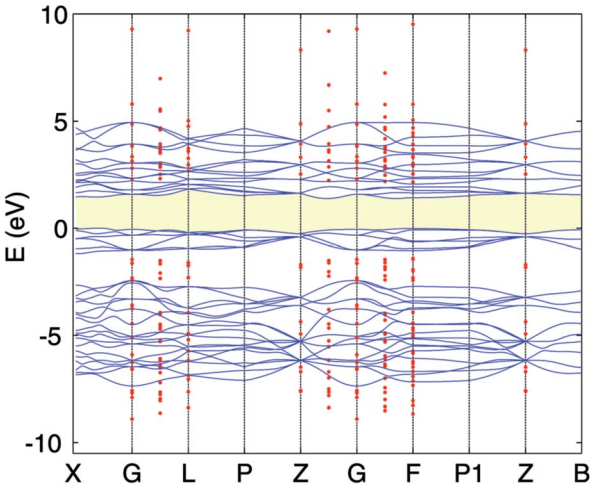

Fig. 4 PBE band structure (full blue line) and $scGW_0$ (red dots) for Cr_2O_3. The VBM of the PBE is set to 0.

width, and second gap, we conclude that $scGW_0$ on top of PBE as well as HSE06 provide sound electronic structure and band gap values. Therefore, we use these approaches to obtain the band gap in the case of $Cr_4S_xO_{6-x}$.

3.2 Anion alloying with sulfur

We find that substituting oxygen with sulfur atoms changes the crystal structure from corundum to monoclinic. As can be seen in Fig. 1 in the case of $x = 2$ the new structure is slightly distorted from the rhombohedral structure. The structural parameters are given in the two first columns of Table 3. First, we must find out for which concentration of sulfur we can expect to have at the same time a low hole mass and large enough gap for transparency. Given the several cases to consider ($x = 1$–5), we employ the PBE+U functional, which is more accurate than the PBE functional. Furthermore, it is known that PBE+U generally gives good values for the effective mass of semiconductors compared to experiment.[51] Our results show that sulfur expands the volume of the corresponding unit cell, as can be expected. Fig. 5 shows the calculated spin polarized band structures of $Cr_4S_xO_{6-x}$ using the PBE+U approximation. For this we used $U_{Cr_d} = 3$ eV and $U_{O_p} = 5$ eV as before. To determine the possible effect of using a U value for sulfur, we performed calculations using $U = 0$ and $U = 5$ eV for the sulfur atom. We found a small difference in DOS and band structures in the case of Cr_2SO_2. For instance, the difference in direct band gap is 0.06 eV (1.77 eV with $U = 5$ *vs.* 1.71 eV with $U = 0$). We expect the difference to be similarly small for the other sulfur concentrations. We therefore use $U = 0$ eV for the sulfur atom in all of our PBE+U calculations.

As can be seen in Fig. 5, increasing the concentration of sulfur atoms increases the dispersion of the VBM, *i.e.* lowers the hole mass, while closing the gap (the values of the fundamental band gaps are listed in Table 3). The blue (grey) curves in each panel show the band structure corresponding to spin up (down). In the case of $Cr_4S_2O_4$ as well as Cr_2O_3, time-reversal symmetry is preserved, therefore the eigenvalues present Kramers degeneracy. But in the other concentrations, since that symmetry is broken, the band structure for up and down spin differ significantly. Inclusion of sulfur increases the magnetic moment of the Cr atoms. The calculated Cr magnetic moments are shown in Table 3 for the different concentrations. The magnetic moments for the other atoms are negligible. Cr_4S_x-O_{6-x} generally presents AFM order, except for $x = 3$ ($Cr_4S_3O_3$), in which case the order is ferrimagnetic, with a total magnetic moment of -0.01 μ_B.

For a good p-type TCO, an optical band gap larger than 3 eV and a low hole effective mass are two critical key properties. Considering the PBE+U band gaps and VBM dispersions for the different concentrations of sulfur, we find that $Cr_4S_2O_4$ presents the best chance for finding a good p-type TCO host among those compounds. Indeed, the PBE+U band gaps for $x > 2$ are too low to expect that a more accurate calculation will results in a gap above 3 eV.

In the next subsection we take a more careful look at the band gap and electronic properties of $Cr_4S_2O_4$.

3.3 $Cr_4S_2O_4$: a new p-type TCO host

In this section we calculate the structural, electronic and magnetic properties of $Cr_4S_2O_4$ using the more accurate HSE06 and $scGW_0$ approaches. There are two different configurations

Table 3 Optimized lattice parameters in Å and α, β, γ in deg, magnetic moment in μ_B, and fundamental band gap E_g in eV of $Cr_4S_xO_{6-x}$, calculated using the PBE+U ($U_{Cr_d} = 3$ eV, $U_{O_p} = 5$ eV) method

Compound	a, b, c	α, β, γ	μ	E_g
Cr_4SO_5	5.38, 5.55, 5.55	55.92, 54.55, 54.55	±2.93, ±2.99	1.92
$Cr_4S_2O_4$	6.08, 5.65, 5.65	57.31, 54.56, 54.56	±3, ±3	1.66
$Cr_4S_3O_3$	6.21, 5.75, 6.04	56.66, 54.11, 55.41	3, −2.98, −3.04, 3.06	1.08
$Cr_4S_4O_2$	6.37, 6.16, 6.16	55.72, 54.02, 54.02	±2.99, ±3.09	0.9
$Cr_4S_5O_1$	6.43, 6.25, 6.43	55.76, 54.44, 55.76	±3.04, ±3.08	0.74

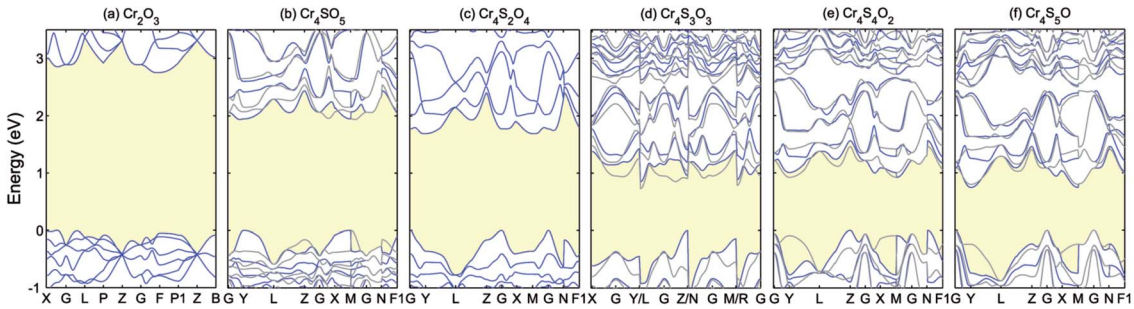

Fig. 5 Band structures of $Cr_4S_xO_{6-x}$ ($x = 0-5$) calculated using PBE+U ($U_{Cr_d} = 3$ eV, $U_{O_p} = 5$ eV). The blue and grey curves show the spin up and down. The VBM is aligned to 0.

when susbstituting two oxygen atoms with sulfur atoms: (i) replacing two S atoms on opposite planes by O (atoms a and c) and (ii) on the same plane (atoms a and b) (see Fig. 1(b)). We found that the first configuration is considerably more stable energetically, with an energy difference of 0.83 eV. Table 4 presents the optimized lattice parameters, magnetic moments and direct band gaps of $Cr_4S_2O_4$ obtained using the HSE06 and $scGW_0$ approaches. PBE and PBE+U results are included for completeness (for the $scGW_0$ calculations we use the PBE lattice parameters). The results show that the HSE06 band gap is close to the $scGW_0$ gap (the difference being 0.19 eV). This indicates that the HSE06 ($\alpha = 0.25$) electronic structure is reliable. In Fig. 6, we show the band structure of $Cr_4S_2O_4$ calculated using (a) PBE+U and (b) HSE06. This shows that the valence band dispersions from the two methods are very similar. We therefore calculate the hole mass of $Cr_4S_2O_4$ using the PBE+U method. We find that the average hole effective mass at the VBM is 1.8 m_e in the directions of G–X and M–G.

Table 4 Optimized lattice parameters (a and b) in Å and α, β in deg, magnetic moment in μ_B, and direct band gap (E_g) in eV of the $Cr_4S_2O_4$ bulk, calculated using different methods

Method	a, b	α, β	μ	E_g
PBE	5.96, 5.62	56.77, 53.68	±2.55	1.09
PBE+U ($U_{Cr_d} = 3$ eV, $U_{O_p} = 5$ eV)	6.08, 5.65	57.31, 54.56	±3	1.77
HSE06 ($\alpha = 0.25$)	6.00, 5.58	57.28, 54.55	±2.95	2.89
$scGW_0$	5.96, 5.62	56.77, 53.68	±2.66	3.08

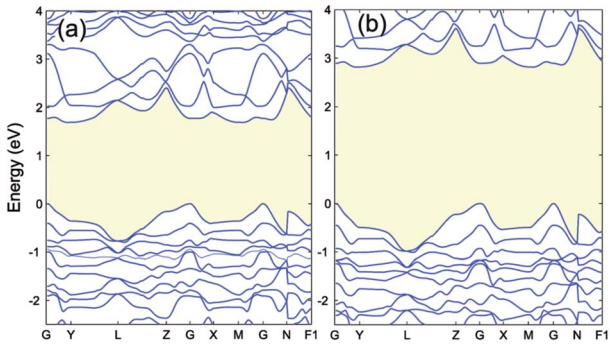

Fig. 6 The band structure of $Cr_4S_2O_4$ calculated by (a) PBE+U ($U_{Cr_d} = 3$ eV, $U_{O_p} = 5$ eV) and (b) HSE06. The VBM is aligned to 0.

The effect of sulfur on the electronic structure can be better understood as follows. The total EDOS and the Cr 3d, O 2p and S 3p partial PEDOS calculated with (a) PBE+U and (b) HSE06 are shown in Fig. 7. We can divide the valence region into the two energy regions. The first region, with -7 eV $< E < -2.8$ eV, consists mainly of O 2p and Cr 3d electrons, with a smaller contribution from S 3p (PBE+U and HSE06 show almost the same contribution). The second region, close to the valence band maximum, with -2.8 eV $< E < 0$, shows the Cr 3d electrons play the leading role, with a smaller mixing of O 2p and S 3p electrons. The conduction band minimum (CBM) is mainly composed of Cr 3d electrons with very small contributions from O 2p and S 3p electrons. The partial density of states shows a significant mixing of O 2p and S 3p toward the VBM. This leads to delocalization of the hole states and increasing the dispersion of the VBM compared to Cr_2O_3 (see Fig. 8). The higher VBM dispersion leads to significantly smaller hole mass, 1.8 m_e compared to 13 m_e in Cr_2O_3 (*i.e.*, more than 7 times smaller). An equally large increase in mobility can be expected. Furthermore, in Fig. 8 we align the Cr_2O_3 and $Cr_4S_2O_4$ PEDOS according to the position of the O 2s level. This shows that replacing oxygen with sulfur shifts the VBM upwards and is the

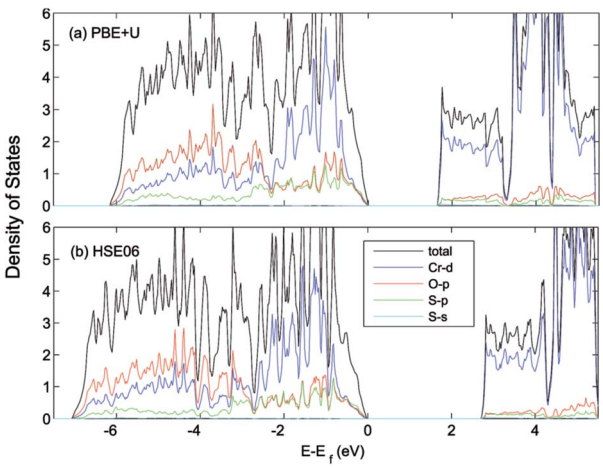

Fig. 7 Total (states per eV per unitcell) and partial (states per eV per atom) density of states of $Cr_4S_2O_4$ calculated using (a) PBE+U ($U_{Cr_d} = 3$ eV, $U_{O_p} = 5$ eV) (b) HSE06 methods. The VBM is aligned to 0.

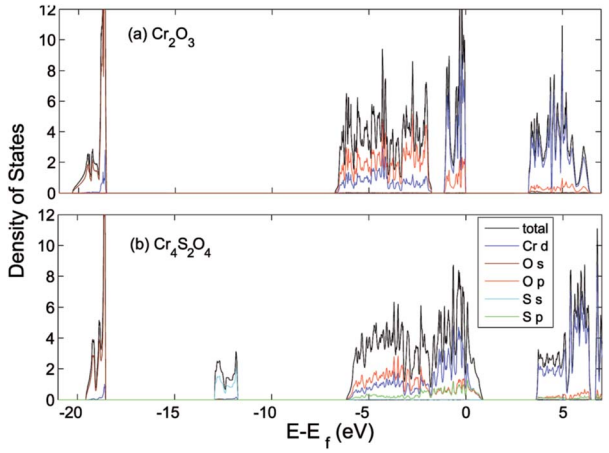

Fig. 8 Total (states per eV per unitcell) and partial (states per eV per atom) density of states of (a) Cr_2O_3 and (b) $Cr_4S_2O_4$ calculated using HSE06. The VB is aligned to the O 1s orbital.

main reason for the band gap decrease with sulfur alloying. On the other hand, a higher VBM (smaller ionization potential) should make p-type dopability easier.[3]

We now address the stability of $Cr_4S_2O_4$. We obtained the mixing enthalpy ΔH from the calculated total energy of each compound[52]

$$\Delta H = 3E_{tot}(Cr_4S_2O_4) - 4E_{tot}(Cr_2O_3) - 2E_{tot}(Cr_2S_3) \quad (1)$$

We found a mixing enthalpy of 144 meV per atom. The positive ΔH indicates that the ground state of $Cr_4S_2O_4$ at zero temperature corresponds to phase separation to Cr_2O_3 and Cr_2S_3. However, at finite temperatures, the mixing entropy will tend to stabilize $Cr_4S_2O_4$. Note, however, that the lattice mismatch between Cr_2O_3 and Cr_2S_3 is large nearly 23%. This is one of the main reasons why the mixing enthalpy above is high. But this large lattice mismatch can be exploited to stabilize $Cr_4S_2O_4$. Indeed, if grown on suitable substrate (*e.g.* by epitaxy), phase separation can be avoided because of this would require overcoming high kinetic energy barriers.[53] Al_2O_3 and stainless steel are popular substrates used to grow Cr_2O_3.[18,54,55] These materials can also be appropriate substrates for $Cr_4S_2O_4$. For instance, Al_2O_3 in its trigonal phase[56] has only 4% lattice mismatch with $Cr_4S_2O_4$ and is thus a reasonable candidate. Stainless steel is composed of different oxides, *i.e.* Cr, Fe, Ni, Co, and depending on growth conditions the surface can be covered by one of the oxides. In the case of, for example, Fe_2O_3 which has the same structure as Cr_2O_3 (corundum) and similar lattice constant (2% different) with $Cr_4S_2O_4$, stainless steel could be a good candidate as well. Note, however, that deciding on a substrate requires the latter to have not only appropriate lattice constant but also suitable electronic and thermodynamic properties. This requires further works going beyond the scope of this paper.

4 Concluding remarks

We investigated the possibility of improving the properties of Cr_2O_3 as a p-type TCO host by anion alloying with sulfur. We employed different DFT approaches, namely PBE, PBE+U, HSE06, as well as GW approximation methods, in order to obtain the structural, electronic and magnetic properties of both pristine Cr_2O_3 and sulfur-alloyed $Cr_4S_xO_{6-x}$ ($x = 1$–5). We demonstrated that substituting oxygen atoms with sulfur can overcome the issue of the flat VBM in Cr_2O_3 and induce a highly-curved VBM, while preserving the transparency. Indeed, we found that $Cr_4S_2O_4$ is the best candidate among the sulfur concentrations considered, with an optical band gap of 3.08 eV and average effective hole mass of 1.8 m_e. Although the stability of this material has not yet being confirmed experimentally, we think our study presents an incentive for future theoretical and experimental works.

Acknowledgements

This work was supported by SIM vzw, Technologiepark 935, BE-9052 Zwijnaarde, Belgium, within the InterPoCo project of the H-INT-S horizontal program. The computational resources and services used in this work were provided by the Vlaams Supercomputer Centrum (VSC) and the HPC infrastructure of the University of Antwerp.

References

1 S. Nandy, A. N. Banerjee, E. Fortunato and R. Martins, *Reviews in Advanced Sciences and Engineering*, 2013, **2**, 132.
2 E. Fortunato, P. Barquinha and R. Martins, *Adv. Mater.*, 2012, **24**, 2945.
3 H. Hosono, *Thin Solid Films*, 2007, **515**, 6000–6014.
4 H. Kawazoe, M. Yasukawa, H. Hyodo, M. Kurita, H. Yanagi and H. Hosono, *Nature*, 1997, **398**, 939.
5 K. Ueda, T. Hase, H. Yanagi, H. Kawazoe, H. Hosono, H. Ohta, M. Orita and M. Hirano, *J. Appl. Phys.*, 2001, **89**, 1790.
6 N. Duan, A. W. Sleight, M. K. Jayaraj and J. Tate, *Appl. Phys. Lett.*, 2000, **77**, 1325.
7 M. Snure and A. Tiwari, *Appl. Phys. Lett.*, 2007, **91**, 092123.
8 R. Nagarajan, A. D. Draeseke, A. W. Sleight and J. Tate, *J. Appl. Phys.*, 2001, **89**, 8022.
9 P. P. Edwards, A. Porch, M. O. Jones, D. V. Morgan and R. M. Perks, *Dalton Trans.*, 2004, **19**, 2995.
10 M. Dekkers, G. Rijnders and D. H. A. Blank, *Appl. Phys. Lett.*, 2007, **90**, 021903.
11 E. Bobeico, E. Varsano, C. Minarini and F. Roca, *Thin Solid Films*, 2003, **70**, 444.
12 N. Uekawa and K. Kaneko, *J. Phys. Chem.*, 1996, **100**, 4193.
13 G. M. Crosbie, G. J. Tennenhouse, R. P. Tischer and H. S. Wroblowa, *J. Am. Ceram. Soc.*, 1984, **67**, 498.
14 K. Hauffe and J. Block, *Z. Phys. Chem.*, 1951, **198**, 232.
15 W. C. Hagel, *J. Appl. Phys.*, 1965, **36**, 2586.
16 P. Qin, G. Fang, Q. He, N. Sun, X. Fan, Q. Zheng, F. Chen, J. Wan and X. Zhao, *Sol. Energy Mater. Sol. Cells*, 2011, **95**, 1005.
17 P. Qin, G. Fang, N. Sun, X. Fan, Q. Zheng, F. Chen, J. Wan and X. Zhao, *Thin Solid Films*, 2011, **519**, 4334.

18 L. Farrell, K. Fleischer, D. Caffrey, D. Mullarkey, E. Norton and I. V. Shvets, *Phys. Rev. B: Condens. Matter Mater. Phys.*, 2015, **91**, 125202.
19 E. Arca, K. Fleischer and I. V. Shvets, *Appl. Phys. Lett.*, 2011, **99**, 111910.
20 E. Arca, K. Fleischer, S. A. Krasnikov and I. Shvets, *J. Phys. Chem. C*, 2013, **117**, 219017.
21 A. Y. Dobin, W. H. Duan and R. M. Wentzcovitch, *Phys. Rev. B: Condens. Matter Mater. Phys.*, 2000, **62**, 11997.
22 R. H. Misho and W. A. Fattahallah, *Thin Solid Films*, 1989, **169**, 235–239.
23 A. B. Kehoe, A. Elisabetta, D. O. Scanlon, I. V. Shvets and G. W. Watson, *J. Phys.: Condens. Matter*, 2016, **28**, 125501.
24 S. Lany, *J. Phys.: Condens. Matter*, 2015, **27**, 283203.
25 P. E. Blöchl, *Phys. Rev. B: Condens. Matter Mater. Phys.*, 1994, **50**, 17953.
26 G. Kresse and J. Hafner, *Phys. Rev. B: Condens. Matter Mater. Phys.*, 1993, **47**, 558.
27 G. Kresse and J. Hafner, *J. Phys.: Condens. Matter*, 1994, **6**, 8245.
28 G. Kresse and J. Furthmller, *Phys. Rev. B: Condens. Matter Mater. Phys.*, 1996, **54**, 11169.
29 G. Kresse and J. Furthmller, *Comput. Mater. Sci.*, 1996, **6**, 1550.
30 J. Perdew, K. Burke and M. Ernzerhof, *Phys. Rev. Lett.*, 1996, **77**, 3865.
31 S. L. Dudarev, G. A. Botton, S. Y. Savrasov, C. J. Humphreys and A. P. Sutton, *Phys. Rev. B: Condens. Matter Mater. Phys.*, 1998, **57**, 1505.
32 V. Stevanovic, S. Lany, X. Zhang and A. Zuner, *Phys. Rev. B: Condens. Matter Mater. Phys.*, 2012, **85**, 115104.
33 A. Rohrbach, J. Hafner and G. Kresse, *Phys. Rev. B: Condens. Matter Mater. Phys.*, 2004, **70**, 125426.
34 J. Heyd, G. E. Scuseria and M. Ernzerhof, *J. Chem. Phys.*, 2003, **118**, 8207.
35 A. V. Krukau, O. A. Vydrov, A. F. Izmaylov and G. E. Scuseria, *J. Chem. Phys.*, 2006, **125**, 224106.
36 L. Hedin, *Phys. Rev. A*, 1965, **139**, 796.
37 M. Shishkin and G. Kresse, *Phys. Rev. B: Condens. Matter Mater. Phys.*, 2006, **74**, 035101.
38 M. Shishkin and G. Kresse, *Phys. Rev. B: Condens. Matter Mater. Phys.*, 2007, **75**, 235102.
39 H. Schober, T. May, B. Dorner, D. Strauch, U. Steigenberger and Y. Morrii, *Z. Phys. B: Condens. Matter*, 1995, **98**, 197.
40 L. Finger and R. Hazen, *J. Appl. Phys.*, 1980, **51**, 5362.
41 M. Catti, G. Sandrone, G. Valerio and R. Dovesi, *J. Phys. Chem. Solids*, 1996, **57**, 1735.
42 B. N. Brockhouse, *J. Chem. Phys.*, 1953, **21**, 961.
43 C. G. Shull, W. A. Strauser and E. O. Wollan, *Phys. Rev.*, 1951, **83**, 333; T. G. Worton, R. M. Brugger and R. B. Bewman, *J. Phys. Chem. Solids*, 1968, **29**, 435.
44 L. M. Corliss, *et al.*, *J. Appl. Phys.*, 1965, **36**, 1099.
45 E. A. Moore, *Phys. Rev. B: Condens. Matter Mater. Phys.*, 2007, **76**, 195107.
46 R. Zimmermann, P. Steiner and S. Hafner, *J. Electron Spectrosc. Relat. Phenom.*, 1996, **78**, 49.
47 T. C. Kaspar, S. E. Chamberlin, M. E. Bowden, R. Colby, V. Shutthanandan, S. Manandhar, Y. Wang, P. V. Sushko and S. A. Chambers, *J. Phys.: Condens. Matter*, 2014, **26**, 135005.
48 F. Werfel and O. Brmmer, *Phys. Scr.*, 1983, **28**, 926.
49 T. Uozumi, K. Okada, A. Kotani, R. Zimmermann, P. Steiner, S. Hfner, Y. Tezuka and S. Shin, *J. Electron Spectrosc. Relat. Phenom.*, 1997, **83**, 920.
50 Y. Guo, S. J. Clark and J. Robertson, *J. Phys.: Condens. Matter*, 2012, **24**, 325504.
51 O. Neufeld and M. Caspary Toroker, *J. Chem. Phys.*, 2016, **144**, 164704.
52 S. H. Wei and A. Zunger, *J. Appl. Phys.*, 1995, **78**, 6.
53 The lattice mismatch between $Cr_4S_2O_4$ and Cr_2O_3, and Cr_2S_3 is as follows: $(\bar{a}_{Cr_4S_2O_4} - a_{Cr_2O_3})/a_{Cr_2O_3} = 7\%$ and $(\bar{a}_{Cr_4S_2O_4} - a_{Cr_2S_3})/a_{Cr_2S_3} = 13\%$, where $\bar{a}_{Cr_4S_2O_4}$ is the average of lattice parameters of $Cr_4S_2O_4$, *i.e.* $a = 6$ Å, $b = 5.58$ Å, and $c = 5.58$ Å. The lattice parameters of Cr_2O_3 and Cr_2S_3 are $a = 5.366$ Å and $a = 6.61$ Å respectively. Note that the above are HSE06 values.
54 S. A. Chambers, Y. Liang and Y. Gao, *Phys. Rev. B: Condens. Matter Mater. Phys.*, 2000, **61**, 13223–13229.
55 R. C. KU and W. L. Winterbottom, *Thin Solid Films*, 1985, **127**, 241–256.
56 A. Jain, S. P. Ong, G. Hautier, W. Chen, W. D. Richards, S. Dacek, S. Cholia, D. Gunter, D. Skinner, G. Ceder and K. A. Persson, *APL Mater.*, 2013, **1**(1), 011002.